A&A 467, L41–L44 (2007)
DOI: 10.1051/0004-6361:20077391

Astronomy & Astrophysics

Letter to the Editor

GRB blastwaves through wind-shaped circumburst media

Z. Meliani[1] and R. Keppens[2,1,3]

[1] FOM-Institute for Plasma Physics Rijnhuizen, PO Box 1207, 3430 BE Nieuwegein, The Netherlands
e-mail: meliani@rijnh.nl
[2] Centre for Plasma Astrophysics, KU Leuven, Belgium
e-mail: Rony.Keppens@wis.kuleuven.be
[3] Astronomical Institute, Utrecht University, The Netherlands

Received 2 March 2007 / Accepted 4 April 2007

ABSTRACT

Context. A significant fraction of progenitors for long gamma-ray bursts (GRBs) are believed to be massive stars. The investigation of long GRBs therefore requires modeling the propagation of ultra-relativistic blastwaves through the circumburst medium surrounding massive stars. We simulate the expansion of an isotropic, adiabatic relativistic fireball into the wind-shaped medium around a massive GRB progenitor. The circumburst medium is composed of a realistically stratified stellar wind zone up to its termination shock, followed by a region of shocked wind characterized by a constant density.
Aims. We followed the evolution of the blastwave through all its stages, including the extremely rapid acceleration up to a Lorentz factor 75 flow, its deceleration by interaction with stellar wind, its passage of the wind termination shock, until its propagation through shocked wind.
Methods. We used the adaptive mesh refinement versatile advection code to follow the evolution of the fireball, from 3.3 s after its initial release up to more than 4.5 days beyond the burst.
Results. We show that the acceleration from purely thermal to ultra-relativistic kinetic regimes is abrupt and produces an internally structured blastwave. We resolved the structure of this ultra-relativistic shell in all stages, thanks to the adaptive mesh. We comment on the dynamical roles played by forward and reverse shock pairs in the phase of interaction with the free stellar wind and clearly identify the complex shock-dominated structure created when the shell crosses the terminal shock.
Conclusions. We show that in our model where the terminal shock is taken relatively close to the massive star, the phase of self-similar deceleration of Blandford-McKee type can only be produced in the constant-density, shocked wind zone.

Key words. gamma rays: bursts – hydrodynamics – ISM: jets and outflows – methods: numerical – relativity – shock waves

1. Motivation

There is increasing evidence that the long-duration ($t_{\rm GRB} > 2$ s) gamma-ray burst (GRB) is associated with the collapse of a massive star with $M \geq 20\ M_\odot$ (Larsson et al. 2007). This evidence is supported by the association of some GRBs with a supernova (Galama et al. 1998; Woosley & Bloom 2006), and also by the association of GRBs with massive star-forming regions in distant galaxies (Wijers et al. 1998; Trentham et al. 2002). As known for supernova blastwave modeling, the surroundings of the exploding stars can influence its propagation. Furthermore, some radio and optical observations are consistent with a scenario of GRB ejecta expanding into a CircumBurst Medium (CBM) with a wind density profile $\rho \propto r^{-2}$ (Panaitescu & Kumar 2004). Since massive stars have significant mass-loss rates and structured wind-blown bubbles surrounding their wind zone, we here investigate the ejecta dynamics as it propagates through the bubble.

Recently, significant progress has been made in investigating the dynamics of ultra-relativistic blastwaves expanding in the CBM of a Wolf-Rayet (WR) star using analytical modeling (Pe'er & Wijers 2006) and by numerical means, exploiting a Lagrangian relativistic hydro code (Nakar & Granot 2006). We complement these efforts here by a numerical simulation of the complete fireball dynamics, expanding in the structured CBM of a WR star. We use grid-adaptive computations with AMRVAC (Keppens et al. 2003) to investigate the ultra-relativistic hydrodynamic evolution of the fireball from its initial purely "hot" phase, up to times significantly beyond its interaction with the transition from free-wind to shocked-wind zones. To make a grid-adaptive computation even feasible, this wind termination shock is supposed to already occur at $R \sim 10^{16}$ cm, which is close to the progenitor compared to values given by models of WR evolution by Castor et al. (1975). Since the radius of a WR star is within the order $3-11\ R_\odot$ (Meynet et al. 2006), this still turns into a need to resolve ultra-relativistic blastwave dynamics over a distance of at least 6 orders of magnitude. Van Marle et al. (2006) explored a number of physical mechanisms that could explain a more restricted free-wind region, such as a high interstellar density and/or pressure, or a lower mass loss rate of the WR star. One of the aims of this paper is to quantify the effect of a sudden, termination-shock variation in the CBM density profile on the dynamics of the blastwave. Some scenarios suggest reproducing the peculiar light-curve evolution of some GRBs (e.g. 990123, 021211, 050904) (Panaitescu & Kumar 2004; Gendre et al. 2007) by invoking an encounter of the blastwave with the density jump across the wind termination shock. This can lead to a brief brightening of the afterglow (Wijers 2001). In such a scenario, the fireball expands during the first hours in a free-wind medium, and after several hours (or few days), the blast further decelerates in shock-dominated interactions with the constant density medium representing shocked wind (Gendre et al. 2007). Before modeling the effects of such

an encounter on the spectral changes in the light curve, we here model the high energy dynamics associated with this terminal shock encounter. We investigate this for the first time numerically for blastwaves in CBM of massive stars.

2. The circumburst medium

Wolf-Rayet stars are possible progenitors GRB. During the WR phase, a massive star with mass $M \geq 20\ M_\odot$ has a mass-loss rate of $\dot{M}_{\rm wind} = 10^{-6}$ to $10^{-4}\ M_\odot$/yr and a fast supersonic wind with speeds of $v_{\rm wind} = 1000$ to 2500 km s^{-1} (Chiosi & Maeder 1986). This wind interacts strongly with the surrounding medium, creating two shocks. At the forward shock, the ambient medium is swept up, where it gets compressed and heated. The reverse shock decelerates the wind itself, and converts almost all the kinetic energy of the wind to thermal energy, producing a hot gas with sound speed on the order of the free-wind speed (Weaver et al. 1977). The two shocked regions are separated by a contact discontinuity, where Rayleigh-Taylor instabilities develop and lead to mixing. The shocked ISM is very dense and cools quickly (Franco et al. 1994). However, the density in the shocked wind zone is lower, so its cooling time is longer. The result is an innermost zone with a hypersonic stellar wind and a second hot and almost isobaric region. It consists of shocked stellar wind, mixed with swept-up ISM. In fact, the total mass in this shocked wind region alone is dominated by mass mixed in and evaporated from the shocked ISM ahead of the contact discontinuity. Still, most swept-up ISM is concentrated in a third region between contact discontinuity and forward shock, where it forms a thin, dense, cold shell. The mass in this thin shell remains dominant throughout the stellar-wind bubble evolution (Weaver et al. 1977). A fourth region is the undisturbed interstellar medium.

The density profile in the free stellar wind is set to $n_{\rm wind}(r) = \dot{M}_{\rm wind}/(4\,\pi v_{\rm wind} r^2 m_{\rm p})$. Here, $m_{\rm p}$ is the mass of the proton. The shocked wind region is isobaric as the sound speed in this region is higher than the speed of expansion of the bubble, i.e. higher than the speed of the forward shock (Castor et al. 1975; Weaver et al. 1977). In this case, the swept-up shell of ambient medium is driven by the pressure of the shocked wind. The pressure in this shocked wind region is then calculated at time t from

$$p_{\rm eq,b} = \frac{7}{(3850\,\pi)^{2/5}} \left(\frac{\dot{M}_{\rm wind}\, v_{\rm wind}^2\, \rho_{\rm ISM}^{3/2}}{t^2} \right)^{2/5}, \quad (1)$$

and the radius of the bubble is computed from

$$R_{\rm FS,wind} = \left(\frac{250}{308\pi} \right)^{1/5} \left(\frac{\dot{M}_{\rm wind}\, v_{\rm wind}^2\, t^3}{\rho_{\rm ISM}} \right)^{1/5}. \quad (2)$$

In these expressions, we introduced the density of the surrounding ISM $\rho_{\rm ISM}$.

The transition from free to shocked wind is at the location of the reverse shock, and this is given by the balance between the thermal pressure in the shocked wind region and the wind ram pressure (true in the case of the energy driven phase when the shocked wind region cools slowly). The strong shock condition at the reverse shock $3v_{\rm wind}^2 \rho_{\rm wind,eq}/4 = p_{\rm eq}$ supposes that the pressure in the shocked wind region is much higher than in the far free wind. This leads to

$$R_{\rm RS,wind} = \left(\frac{3}{4} \frac{\dot{M}_{\rm wind} v_{\rm wind}}{4\pi p_{\rm eq,b}} \right)^{1/2} \propto \left(\frac{\dot{M}_{\rm wind}^3 v_{\rm wind} t^4}{\rho_{\rm ISM}^3} \right)^{1/10}. \quad (3)$$

In the following, we model the fireball expanding through only the free-wind and part of the shocked wind region. Our wind termination shock will be at about 10^{16} cm, in accordance with Eq. (3) for a high-density surrounding medium with $\rho_{\rm ISM} = m_{\rm p} 10^5$ cm^{-3}, a short WR lifetime $t_{\rm WR} = 100$ year, a mass loss in the wind of $\dot{M}_{\rm wind} = 10^{-6}\ M_\odot$/yr, and wind speed $v_{\rm wind} = 10^3$ km s^{-1}. While the last two are typical values in some circumburst media for GRB (Arthur 2006), we took a very short WR lifetime to investigate the case where the terminal shock is at a much shorter distance than the typical 1 pc (Chevalier et al. 2004). The density profile of the CBM in our model is given in Fig. 1. The pressure profile in the free supersonic stellar wind is deduced by considering a Mach number $\mathcal{M} = 3$. The wind is then cold, and its pressure will have no effect on the propagation of the fireball. In the shocked wind, the constant pressure is given by Eq. (1), while the constant density is increased fourfold in accordance with the strong shock requirement. The wind velocity is constant throughout the wind zone and neglected in the shocked wind region. This is a proxy for the reduction by a factor of 4 expected at the termination shock.

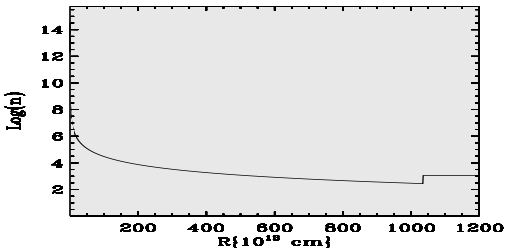

Fig. 1. The density profile of the CBM in our model.

3. GRB shell model and evolution

Initially we set a uniform static and hot shell that extended up to radius $R_0 = 10^{11}$ cm. The initial specific enthalpy, normalized to c^2, in the uniform shell is $\bar{\eta}_{\rm sh} = 100$, and its energy is

$$E_{\rm sh} = 10^{51}\ {\rm erg} = 4\pi R_0^2 \delta \bar{\eta}_{\rm sh} c^2 n_{\rm sh} m_{\rm p} \quad (4)$$

where δ stands for the thickness of the shell. We set approximately $\delta \sim c\,\Delta t \sim 10^{11}$ cm, where $\Delta t \approx 3$ s is the duration of the GRB. The mass of the shell is $M_{\rm sh} = E_{\rm sh}/(\bar{\eta}_{\rm sh}\, c^2)$. The shell is static and hot, and the initial pressure is set to $p_{\rm sh} = \frac{\Gamma-1}{\Gamma} n_{\rm sh}\, (\bar{\eta}_{\rm sh} - 1)\ m_{\rm p}\, c^2$ and the density from Eq. (4). Initially, the energy of the shell is only thermal. We use a constant polytropic index $\Gamma = 4/3$, as the temperature of the shell is relativistic and the interaction shell-ISM will be dominated by the forward shock, where the temperature of the shocked ISM is also relativistic. The computation is done on a domain extending from a radius of 10^9 cm to 1.2×10^{16} cm, with the initial shell region between 2×10^9 cm and 10^{11} cm. In the grid-adaptive numerical simulation, we use 1200 grid points on the base grid level, and allow for 15 grid levels in total, with a doubling of the effective resolution between each grid level.

In Fig. 2, we draw the variation in time of the maximum Lorentz factor of the fireball. We also draw the variation of the Lorentz factor at the forward shock alone: this coincides mostly with the instantaneous maximum Lorentz factor, except for those intervals where reverse shock dynamics is particularly prominent, as discussed below. In Fig. 3, we draw the variation of the maximum pressure with time. Note that we translated to comoving (at the forward shock) time for the latter.

In the first phase of the simulated fireball, the initial hot shell and a fraction of swept-up matter are accelerated thermally (Fig. 3) very fast, such that a maximal Lorentz factor of

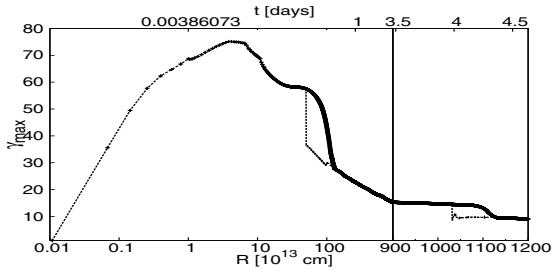

Fig. 2. The variation in the maximum Lorentz factor. We also plot the Lorentz factor at the forward shock. The variation is presented a function of the distance and in the lab-frame time. Note the change from log to linear scale at 9×10^{15} cm.

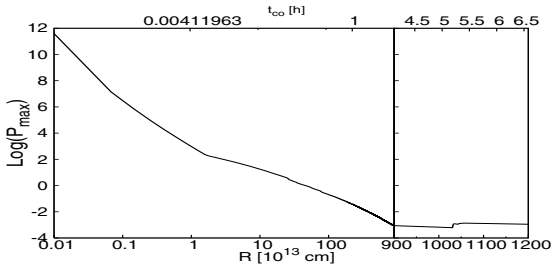

Fig. 3. The variation in the (logarithm of) maximum pressure as a function of the distance and the comoving frame time.

$\gamma_{\max} = 75$ is reached within $t_{\rm acc} \sim 1200$ s (Figs. 2 and 4). As the shell is initially uniform, the center and back of the shell get delayed in their acceleration with respect to the front of the shell, and they reach a lower Lorentz factor and introduce a tail structure (Fig. 4). The maximum Lorentz factor reached is low in the sense that $\gamma_{\max} < \bar{\eta}_{\rm sh} = 100$, due to the influence of accreted mass from the wind. This influence will generally depend on the initial energy in the shell $E_{\rm sh}$ and the mass loss rate in the wind. In the simulation, in this acceleration phase the shell has accreted and accelerates with it a mass of $M_{\rm acc,wind} = 0.024\, M_{\rm sh}$. If the realized energy in the GRB is higher, the maximum Lorentz factor reached by the shell will increase, too.

After this rapid acceleration phase, the swept-up wind mass increases enough to influence the dynamics of the shell. The shell now decelerates by transferring kinetic energy at both a forward and a reverse shock pair. An intermediate contact discontinuity separates shell from the swept-up, shocked wind matter. At the forward shock, the kinetic energy of the shell is passed to a swept-up shocked wind. As the shell has an internal structure produced during the acceleration phase (Fig. 4), the maximum Lorentz factor seen in the evolution (Fig. 2) decreases smoothly. This is contrasts with the sudden change seen in simulations where a uniform shell travels through constant medium density, as discussed in detail by Meliani et al. (2007). In this more realistic case, the reverse shock will cross that frontal part of the shell with the highest Lorentz factor at about time $t \sim 6 \times 10^3$ s. In a second phase, the overall maximal Lorentz factor remains constant $\gamma \sim 58$ until $t \sim 19 \times 10^3$ s. This coincides with those times when the reverse shock crosses the middle part of the shell, which has acquired a constant Lorentz factor.

After this, the reverse shock starts to propagate in the tail of the shell and, in this phase, the reverse shock is mildly relativistic. This lasts in Fig. 2 until $t \sim 9.4$ h marking a relatively fast decrease in the maximum Lorentz factor, which actually coincides with the Lorentz factor in the, as yet, unshocked shell part ahead of the reverse shock. Beyond this rapid phase, the maximum Lorentz factor seen is situated at the front of the forward shock. In this phase more energy starts to be transferred to swept-up, shocked wind matter, and the Lorentz factor at the forward shock decreases with time with a slope smaller than $-1/2$. The latter dependence would be expected from by the analytic Blandford-McKee solution, but in our simulation not all shell energy has already been transferred to accreted matter, which is assumed in the self-similar solution.

When the shock-dominated shell structure finally reaches the wind termination shock $R_{\rm RS,wind}$, all the matter originally in the free-wind zone is swept-up by the shell and compressed between its forward shock and contact discontinuity (Fig. 4). As the forward shock is relativistic (Fig. 4), the compression ratio of the number density there is $\frac{n_2}{n_1} \sim 59.4 \sim (4\gamma(r) + 3)$, where n_2 is the density in the compressed wind matter, while n_1 is the original wind density. Similarly, the thermal energy density in the compressed wind matter is $e_2 \sim (\gamma_2 - 1)\rho_2 c^2$ (Blandford & McKee 1976), which corresponds to analytical estimates. However, as stated above, the shell does not yet reach a self-similar Blandford-McKee phase while traversing the free-wind zone, as the reverse shock continues to propagate in the tail of the shell and not all its energy is transferred to swept-up matter. The Blandford-McKee phase can be reached in a free stellar-wind region when the terminal shock would be faraway. Due to our assumption of a relatively close termination shock, our numerical simulation allows us to investigate blast waves interacting with wind termination shocks before the Blandford-McKee phase.

As soon as the shell structure has encountered the wind termination shock and starts to travel through the shocked wind region, the entire shell is actually composed of multiple regions (Fig. 4). From right to left, we find (1) a forward shock now propagating in the shocked wind region. We then encounter (2) a contact discontinuity separating the re-shocked shocked wind from the swept-up free wind. This wind is shocked once more by (3) a new reverse shock propagating through the already swept-up compressed wind matter. This matter extends to (4) the original contact discontinuity between shell and swept-up wind matter. At this new reverse shock (3), the Lorentz factor falls to $\gamma_3 \sim 10 = 0.725\gamma_2$ and the density increases to $n_3 \sim 28 \times 10^4\,{\rm cm}^{-3} = \sqrt{3}n_2$. Furthermore, the thermal energy $e_3 \sim 2.1 e_2$ and this new reverse shock remains Newtonian until the time $t = 4.16$ day. The relations between the values of the density and Lorentz factor are in good agreement with recent analytical estimates by Pe'er & Wijers (2006). Between (3), the new reverse shock, and (4), the old contact discontinuity, there is at first still a region of the swept-up wind matter with values for $n_2(r)$ (decreased due to spherical expansion) and γ_2 as discussed above. Further leftward of (4) the old contact discontinuity, we find all the initial shell material, separated by (5) the old reverse shock, which continues to propagate in the tail of the initial shell. Hence, there are two regions in this part of the structure as well, namely shocked-shell matter between the contact discontinuity (4) and the initial reverse shock (5), and the original unshocked-shell matter.

The new reverse shock (3) eventually crosses all the region that extends up to the original contact discontinuity (4), and it arrives there at a distance $R_1 \sim 1.1 \times 10^{16}$ cm. For times up to this arrival at R_1, the maximum Lorentz factor seen in Fig. 2 undergoes a weak variation, since the Lorentz factor γ_2, density n_2, and energy in the swept-up wind region vary little. After arrival at R_1, the maximum Lorentz factor drawn in Fig. 2 represents the value in the region of shocked-shell matter ahead of the new reverse (Newtonian) shock, where the Lorentz factor decreases more strongly. After $R > 1130 \times 10^{13}$ cm, the maximum

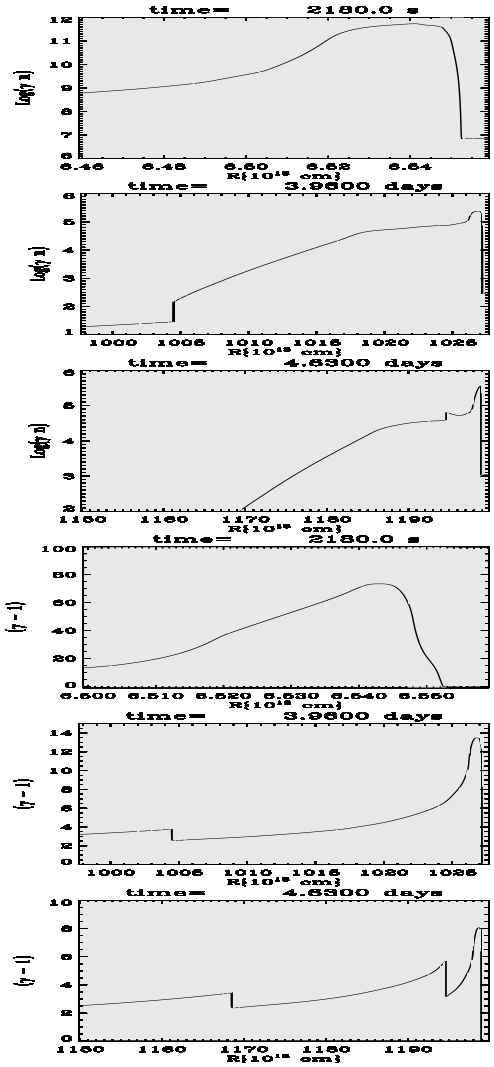

Fig. 4. All zones present when the relativistic shell interacts with the CBM. The shell profile is shown at three different times: from top down: at time t = 2180 s after the rapid thermal acceleration; at time t = 3.96 days, prior to the encounter with the wind termination shock at time t = 4.63 days. The first three frames show the logarithm of density in the lab-frame, the last three show kinetic energy.

Lorentz factor drawn in Fig. 2 starts to represent the value at the forward shock (1) again, in the phase before it reaches the Blandford-McKee phase. From then on, while the new reverse shock continues to propagate through the original shell structure, the maximum Lorentz factor at the forward shock starts to decrease with distance with a slope −0.9. This is still less than the slope in the expected long-term Blandford-McKee phase. To arrive at this phase, a still larger computational domain and a larger simulation time is needed.

In Fig. 2, the time delay in the drop of the maximum Lorentz factor from when the shell crosses the wind terminal shock is thus related to the time for the new reverse shock to propagate through the region (2)−(4). Note that the maximal pressure in Fig. 3 directly increases at the wind terminal shock encounter.

4. Conclusions

In this work, we have investigated all phases of the GRB in a fireball modeled. We model the propagation of the thermal fireball through a complex wind-shaped CBM of a massive star. The fireball interacts with free stellar wind, crosses the wind terminal shock, and then propagates in the shocked wind zone. We discussed initial acceleration, energy transfer to CBM, deceleration, and interaction with the terminal shock. When the shell reaches the wind termination shock, the structure of the shell changes and multiple regions form: a forward shock, two contact discontinuities, and two reverse shocks characterize the evolving structure. We have shown that our simulations agree in terms of compression ratios, Lorentz factors, and energies reached at all these shocks with analytical estimates exploiting the jump conditions (Pe'er & Wijers 2006).

There are pronounced differences in the deceleration as quantified by the variation in the instantaneous maximum Lorentz factor with models of the afterglow phase alone (Meliani et al. 2007). We showed that the rapid thermal acceleration produces a cold shell with internal structure where the Lorentz factor and density decrease from the head to the back of the shell. This has distinct consequences for its further long-term evolution and deceleration. In the deceleration phase before Blandford-McKee, the shell decelerates with a slope −0.9 in the constant density medium. These results obtained using high-resolution numerical simulation bring out important differences with analytical estimates, in particular with respect to the internal structure of the expanding high-energy shell. In future work, the results obtained with our model will be used to deduce light curves, and to show how sudden rebrightenings may help to deduce the position of the terminal shock. We have shown here that it is not appropriate to use the self-similar Blandford-McKee solution around the terminal shock. Future work will explore multi-dimensional scenarios and quantify the spectral outcome.

Acknowledgements. We acknowledge financial support from NWO-E grant 614.000.421 and computing resources by NCF grant SG-06-276 and the VIC cluster at K.U. Leuven.

References

Arthur, S. J. 2006, Diffuse Matter from Star Forming Regions to Active Galaxies – A volume Honouring John Dyson, ed. T. W. Harquist, J. M. Pittard, & S. A. E. G. Falle [arXiv:astro-ph/0605533]
Blandford, R. D., & McKee, C. F. 1976, Physics of Fluids, 19, 1130
Castor, J., McCray, R., & Weaver, R. 1975, ApJ, 200, L107
Chevalier, R. A., Li, Z., & Fransson, C. 2004, ApJ, 606, 369
Chiosi, C., & Maeder, A. 1986, ARA&A, 24, 329
Franco, J., Miller, W. W., Arthur, S. J., Tenorio-Tagle, G., & Terlevich, R. 1994, ApJ, 435, 805
Galama, T., Vreeswijk, P. M., van Paradijs, J., et al. 1998, Nature, 395, 670
Gendre, B., Galli, A., Corsi, A., et al. 2007, A&A, 462, 565
Keppens, R., Nool, M., Tóth, G., & Goedbloed, J. P. 2003, Comp. Phys. Commun., 153, 317
Larsson, J., Levan, A. J., Davies, M. B., & Fruchter, A. S. 2007 [arXiv:astro-ph/0701562]
Meliani, Z., Keppens, R., Casse, F., & Giannios, D. 2007 [arXiv:astro-ph/0701434]
Meynet, G., Mowlavi, N., & Maeder, A. 2006 [arXiv:astro-ph/0611261]
Nakar, E., & Granot, J. 2006 [arXiv:astro-ph/0606011]
Panaitescu, A., & Kumar, P. 2004, MNRAS, 353, 511
Pe'er, A., & Wijers, R. 2006, ApJ, 643, 1036
Trentham, N., Ramirez-Ruiz, E., & Blain, A. W. 2002, MNRAS, 334, 983
Van Marle, A. J., Langer, N., Achterberg, A., & Garcia-Segura, G. 2006, A&A, 460, 105
Weaver, R., McCray, R., Castor, J., Shapiro, P., & Moore, R. 1977, ApJ, 218, 377
Wijers, R. 2001, in Gamma-Ray Bursts in the Afterglow Era, ed. E. Costa, F. Frontera, & J. Hjorth (Springer-Verlag), 306
Wijers, R. A. M. J., Bloom, J. S., Bagla, J. S., & Natarajan, P. 1998, MNRAS, 294, L13
Woosley, S. E., & Bloom, J. S. 2006, ARA&A, 44, 507